Magnetic Refrigeration with Recycled Permanent Magnets and Free Rare-Earth Magnetocaloric La–Fe–Si

Benke, Dimitri; Fries, Maximilian; Specht, Marius et al.

(2020)

Energy Technology
Generation, Conversion, Storage, Distribution
www.entechnol.de

Magnetic Refrigeration with Recycled Permanent Magnets and Free Rare-Earth Magnetocaloric La–Fe–Si

Dimitri Benke, Maximilian Fries, Marius Specht, Jonas Wortmann, Marc Pabst, Tino Gottschall, Iliya Radulov, Konstantin Skokov, Alex Ivor Bevan, Davide Prosperi, Catalina Oana Tudor, Peter Afiuny, Miha Zakotnik, and Oliver Gutfleisch*

Magnetic refrigeration is an upcoming technology that could be an alternative to the more than 100-year-old conventional gas–vapor compression cooling. Magnetic refrigeration might answer some of the global challenges linked with the increasing demands for readily available cooling in almost every region of the world and the global-warming potential of conventional refrigerants. Important issues to be solved are, for example, the required mass and the ecological footprint of the rare-earth permanent magnets and the magnetocaloric material, which are key parts of the magnetic cooling device. The majority of existing demonstrators use Nd–Fe–B permanent magnets, which account for more than 50% of the ecological footprint, and Gd, which is a critical raw material. This work shows a solution to these problems by demonstrating the world's first magnetocaloric demonstrator that uses recycled Nd–Fe–B magnets as the magnetic field source, and, as a Gd replacement material, La–Fe–Mn–Si for the magnetocaloric heat exchanger. These solutions show that it is possible to reduce the ecological footprint of magnetic cooling devices and provides magnetic cooling as a green solid-state technology that has the potential to satisfy the rapidly growing global demands.

1. Introduction

Throughout most of history mankind has been preoccupied with the question of how to keep warm, but in the 21st century, the emphasis has shifted to how to keep us and our environment cool. At present, approximately 17% of the world's electricity is used for various kinds of cooling.[1] However, demand is expected to rise exponentially, from the current 300 TWh in 2000, to approximately 10 000 TWh by 2100.[1] According to a recent study, the energy demand for cooling will exceed the demand for heating in 2070.[1]

At the moment, most of the cooling demand is satisfied by the use of gas–vapor compression devices, a technology that is essentially unchanged for more than 100 years. This technology uses pumps to do the work of compressing the fluid refrigerants (normally hydrofluorocarbons [HFCs]) to absorb and release the heat, but it does this with an efficiency of only about 30% of the Carnot efficiency, i.e., the thermodynamic limit.[2] In addition, most of the refrigeration gases used today have a significant global-warming potential (e.g., the GWP of R-134a is 1430 times higher than that of CO_2) and need to be phased out in accordance with the Kigali agreement.[3] Both the low efficiency of vapor compression and the use of these gases, which can be thought of as catalysts of climate change, will increase the rate of global warming as the demands for cooling increase.

Alternatively, environmental-friendly and energy-efficient technologies need to be developed and implemented quickly to satisfy our demands for more comfortable living conditions. One option is thermoelectric coolers based on the Peltier effect, but these only reach 10% of Carnot efficiency, at best, and will only ever occupy niche markets.[4]

D. Benke, Dr. M. Fries, M. Specht, J. Wortmann, M. Pabst, Dr. T. Gottschall, Dr. I. Radulov, Dr. K. Skokov, Prof. O. Gutfleisch
Material Science
TU Darmstadt
64287 Darmstadt, Germany
E-mail: dimitri.benke@tu-darmstadt.de

The ORCID identification number(s) for the author(s) of this article can be found under https://doi.org/10.1002/ente.201901025.

DOI: 10.1002/ente.201901025

Dr. A. I. Bevan, D. Prosperi, Dr. C. O. Tudor, P. Afiuny, Dr. M. Zakotnik
Urban Mining Company
1550 Clovis Barker Rd., San Marcos, TX 78666, USA

Prof. O. Gutfleisch
Institute for Resource Strategy and Materials Cycles
Fraunhofer IWKS
Hanau, Germany

A more promising alternative is magnetic refrigeration based on the magnetocaloric effect (MCE).[5] MCE technology exploits the temperature change of a ferromagnetic material (the magnetocaloric material) when exposed to a magnetic field change.[6]

With this technology no potentially harmful gaseous refrigerants leak into the atmosphere, and using renewable energy, magnetic cooling can operate with zero global-warming consequences.[7] This means that the MCE is able to give us the best of both worlds: higher efficiency with much less CO_2 being produced and no leakage of gaseous refrigerants into the atmosphere.[3,8]

Of course, the magnetocaloric material in a device must not only have excellent primary magnetocaloric properties, such as a high adiabatic temperature and magnetic entropy changes but also good secondary properties such as corrosion resistance, mechanical stability, and easy machinability.[6] Gadolinium is the most frequently used material in prototypes as it fulfils many of the aforementioned requirements. But its low abundance would become a serious problem as soon as large-scale use of this technology begins to take off.[9]

La–Fe–Mn–Si is a viable alternative to gadolinium, based on its excellent magnetocaloric properties and the high abundance of its constituent elements.[6,9,10] However, the narrow temperature window within which these alloys work poses a serious challenge.[11]

To create a large magnetic field in an efficient way, high-performance magnets with a high remanence and a sufficient coercivity are needed. Using a Halbach array, the potential applied magnetic fields that can act on the magnetocaloric material can exceed 1 T.[12]

Only Nd–Fe–B magnets have a high enough energy density to build cooling devices that are comparable in cooling capacity and temperature span to existing vapor–compressor technology.[7]

However, at the same time, we must consider the economic and ecological implications of using rare-earth (RE)-based magnets. The mining and separation processes associated with these materials detrimentally affect the environment and there are also a number of socioeconomic implications.[13] In fact, the CO_2 emissions during the production process for these magnets can be larger than the potential savings accrued during the lifetime of the magnetocaloric device.[14,15]

To create a truly green cooling technology, it is necessary to build the devices from recycled permanent magnets. This will drastically reduce the environmental impact of the magnets.[14] At the same time, it will also reduce the dependence on mainly Chinese imports of materials, as China controls some 94% of the RE's market share and 75% of the NdFeB magnets globally.[16]

In this article, we present a green magnetic-cooling demonstrator based on recycled Nd–Fe–B magnets and an environmental-friendly magnetocaloric material, La–Fe–Mn–Si that shows a significant temperature span and can be used as a versatile test system for magnetocaloric regenerators.[17]

The article is structured as follows. We start by discussing the prerequisites for the magnetic field source with respect to magnetic cooling and describe the recycling procedure and provide an assessment of the recycled Nd–Fe–B material. Then the magnetocaloric properties of the La–Fe–Mn–Si material are presented. This is followed by a brief description of the design and optimization of our test system. In the following section, we give insights into the utilization of the La–Fe–Mn–Si in our cooling test system. Finally, we summarize the results and answer the question as to whether green magnetic cooling is possible.

2. Magnetic Field Source Based on Recycled Nd–Fe–B Permanent Magnets

Permanent magnets are magnetically "hard" materials that retain their magnetization after the removal of the magnetizing field, independent of their geometry. The most important properties for magnetic refrigeration are the remanent magnetic flux density B_r and the resistance to demagnetization, the coercivity H_c.[7] In general, the MCE scales with the applied magnetic field change.[18] Therefore, the remanent flux density is very important, but we also need to make sure that the permanent magnet is appropriate for the desired operating temperature.

Nd–Fe–B is the best choice of permanent-magnet material as it offers high remanent flux densities, good mechanical properties, and the temperature stability of the remanence and the coercivity can be controlled by doping with additional elements.[5]

The production of Nd–Fe–B magnets that involves the mining of the primary elements is environmentally detrimental: one ton of RE produced, generates approximately 8.5 kg of fluorine and 13 kg of dust; and using concentrated sulfuric acid high-temperature calcination techniques to produce approximately one ton of calcined RE ore generates 9600 to 12 000 cubic meters of waste gas containing dust concentrate, hydrofluoric acid, sulfur dioxide, and sulfuric acid, approximately 75 cubic meters of acidic wastewater, and about one ton of radioactive waste residue (containing water).[19] At the same time, the manufacturers of applications that include permanent magnet are not willing to pay for the sustainable mining of RE elements. A response to this dilemma is to develop technologies to reuse the REs that have already been extracted from the ground.[20–24]

Recycling Nd–Fe–B creates a closed loop and eliminates many of the environmentally damaging aspects of production, e.g., ore mining, acid leaching, and solvent extraction. A common problem with recycling is that the magnetic properties of the Nd–Fe–B material gradually decrease with each cycle of reuse, as oxidation and contamination take their toll. This limits the potential of a system that merely retains the Nd–Fe–B materials' original magnetic properties.[25] However, Urban Mining Company (UMC), operating on a commercial scale, has shown that the Magnet-to-Magnet (M2M) and the Grain-Boundary Engineering (GBE) processes can produce recycled magnets with comparable or improved magnetic performance relative to the first-use magnets produced from mined and refined REs. Therefore, several life cycles of Nd–Fe–B magnets are possible using this method.[25–27]

In this work, recycled magnets from the UMC, USA, processed via GBE, were used and analyzed with respect to their microstructure and magnetic properties and compared with conventional Nd–Fe–B sintered magnets.

2.1. Recycling Procedure

The patented M2M (US8734714B2) process takes scrap Nd–Fe–B-based magnets and recycles them into new magnets while maintaining largely their physical and magnetic properties

or tailoring them to their specific new use. It is also important to note that this process can be repeated multiple times.

The process begins with the Nd–Fe–B magnets harvested from MRI machines, hard-disk drives, electric motors, and loudspeakers.[28] The waste Nd–Fe–B is removed from the End-of-Life (EOL) application, demagnetized, chemically and magnetically characterized, cleaned to remove any residual coating and surface-oxide layer before entering the next stage of process. A specifically designed additive alloy with amounts, for example, 2.0 and 3.0 wt%, is then introduced to engineer the grain-boundary phase to achieve the required magnetic specifications. The additive is a multi-element alloy, with a composition weight percentage of $Nd_6Dy_{21}Co_{19}Cu_{2.5}Fe_{51.5}$[21,25,27,29] that is mixed with the waste feedstock that undergoes a variety of milling and mixing stages, including a coarse milling and homogenizing procedure in a hydrogen-mixing reactor, until it is reduced to a homogenous, uniform composition and a powder size of approximately 3.5 μm (D50) using a jet mill. The powder is then transferred to a mold to be aligned in a magnetic field and pressed along a direction orthogonal to the applied aligning field (**Figure 1**). During this stage, each tiny powder particle, i.e., a magnetic single crystal, orientates itself in the magnetic field so that all the crystals are well-aligned. In the next stage, an isostatic press is applied with a pressure of 200 bar to produce a green compact in the form of a block. The blocks are then vacuum sintered and given a post-sintering heat treatment to produce the fully dense Nd–Fe–B magnets with optimized magnetic properties for subsequent cutting to shape and coating (see Figure 1).

2.2. Microscopic Characterization

The recycling method used by UMC involves mixing the used magnet powder with additives of a RE-rich multi-element alloy, which leads to the GBE of the $Nd_2Fe_{14}B$ main phase. Two different grades of material with different amounts of additives (2 and 3 wt%) were produced and characterized for this study.

The microstructures of the recycled Nd–Fe–B magnets with 2 and 3 wt% additives are shown in **Figure 2** in scanning electron microscopy back-scattered electron (SEM BSE) mode. Our analysis shows the increasing areal fraction of metallic Nd-rich phase (white contrast) with specific additional elements as specified earlier, which helps to form a more uniform grain-boundary phase with excellent wettability and good chemical stability. In addition, a Dy gradient across the grain-boundary phase into the main magnetic phase is responsible for the formation of a shell with a local increase in the magnetocrystalline anisotropy of the $Nd_2Fe_{14}B$ main phase, where it can be most effective. This gradient can be seen in Figure 2 as a bright shell at the edge of the grains. The combined effect of these two features is responsible for the improved thermal stability and coercivity of the recycled magnets. Magnets with higher amounts of additives have more RE-rich phase that separate the grains of the matrix phase. All the magnets are fully dense, and the microstructure is similar to that of conventional magnets made from primary material, and also shows some distinct differences.

Between larger grains that consist of the $Nd_2Fe_{14}B$ main phase, smaller grains of spherical shape with a high RE content

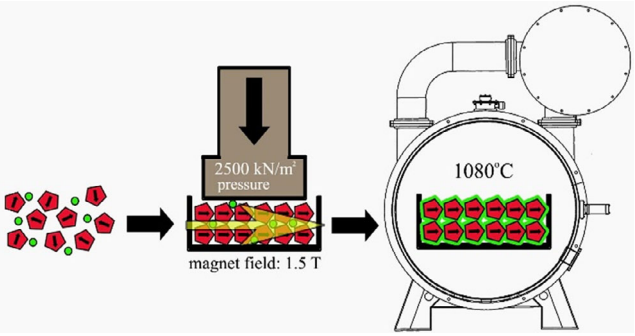

Figure 1. Schematic of the Magnet-to-Magnet recycling process.[21] Waste NdFeB is depicted in red and the specially developed alloy which is added to coat the particles of the initial magnetic alloy in green.

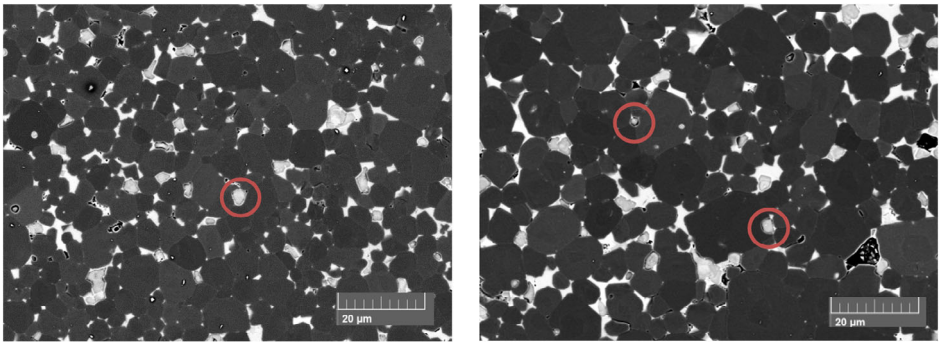

Figure 2. SEM BSE microstructures of recycled sintered NdFeB magnets with different amounts of additive alloy (top 2 wt% and bottom 3 wt% additive alloy). A different Dy/Nd ratio can be found in the particles with the red circle.

can be found (see red circles in Figure 2). These smaller grains have a 3–4 times higher ratio of Dy to Pr and of Dy to Nd than the main phase. This is due to the Dy in the additive alloy that was mixed with the scrap magnets and traces of this process can be found in these smaller grains.

Within the Nd–Fe–B grains, a contrast difference can be observed which indicates a higher RE content on the edges of the grain than in the center. Similar behavior could be observed in the work of Loewe et al.[30] where the grain boundary diffusion of Dy and Tb into Nd–Fe–B was discussed. This could imply that the RE from the added RE-rich additives diffused into the Nd–Fe–B grains forming a RE-rich shell. Overall, the microstructural observations here are consistent with the work of Sepehri–Amin[25] where similar magnets were studied.

The electron backscatter diffraction (EBSD) image in **Figure 3** shows a very good alignment of the larger grains and a minor misalignment of the smaller grains. Overall, a degree of texture of 95% was achieved in this magnet. The color of the grains represents the angle of the c axis of the grains (see inset) and black areas correspond to phases that are not the main phase.

2.3. Magnetic Characterization

Figure 4 shows the demagnetization curves for both materials at room temperature. The magnet with 2 wt% additives shows $\mu_0 M_r = 1.31\,\mathrm{T}$, $\mu_0 H_c = 2.02\,\mathrm{T}$, and a $\mathrm{BH_{max}} = 346\,\mathrm{kJ\,m^{-3}}$; the magnet with 3 wt% additives shows $\mu_0 M_r = 1.30\,\mathrm{T}$, $\mu_0 H_c = 2.35\,\mathrm{T}$, and a $\mathrm{BH_{max}} = 320\,\mathrm{kJ\,m^{-3}}$. These values are comparable with commercially available magnets that contain a similar amount of heavy RE. For example, the magnet grade 42SH from Magnet World has a remanence of 1.3 T, a coercivity of 2 T, and an energy product $328\,\mathrm{kJ\,m^{-3}}$. VACODYM 238 AP from Vacuumschmelze shows a similar performance as well.

Consistent with the basic intrinsic properties of the light- and heavy-RE-based alloys, the materials with larger amounts of additives (which contain larger amounts of heavy REs, see **Table 1**) have a higher coercivity, but a lower remanence.

The inset of Figure 4 shows the temperature-dependent coercivity and remanence of both magnets, which were obtained from the demagnetization curves measured between 20 and 160 °C. The temperature coefficient of remanence (α), coercivity (β), and the maximum energy product (γ) of both magnets were measured from 20 to 150 °C in accordance with the guidelines in IEC-61807.[31]

All results are summarized in Table 1 together with the magnetization at 14 T measured in the PPMS system.

The demagnetizing fields expected in the MCE demonstrator can reach up to 1.2 T. Previous experiments have shown that

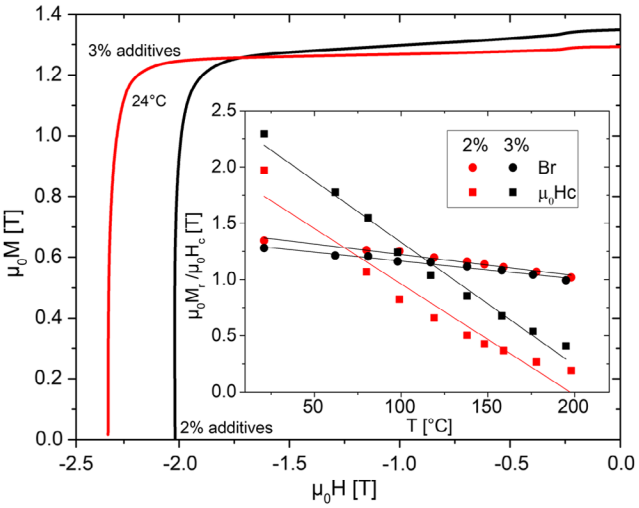

Figure 4. Hysteresis and their temperature dependence of the two different recycled materials.

Table 1. Magnetic properties of the recycled Nd–Fe–B magnets.

Additives [wt%]	2	3
$\mu_0 M_r$ [T]	1.31	1.30
$\mu_0 M(@14T)$ [T]	1.37	1.33
$\mu_0 H_c$ [T]	2.02	2.35
$\mathrm{BH_{max}}$ [kJ m^{-3}]	346	320
α [% K^{-1}]	0.1	0.1
β [% K^{-1}]	0.6	0.6
γ [% K^{-1}]	0.13	0.2

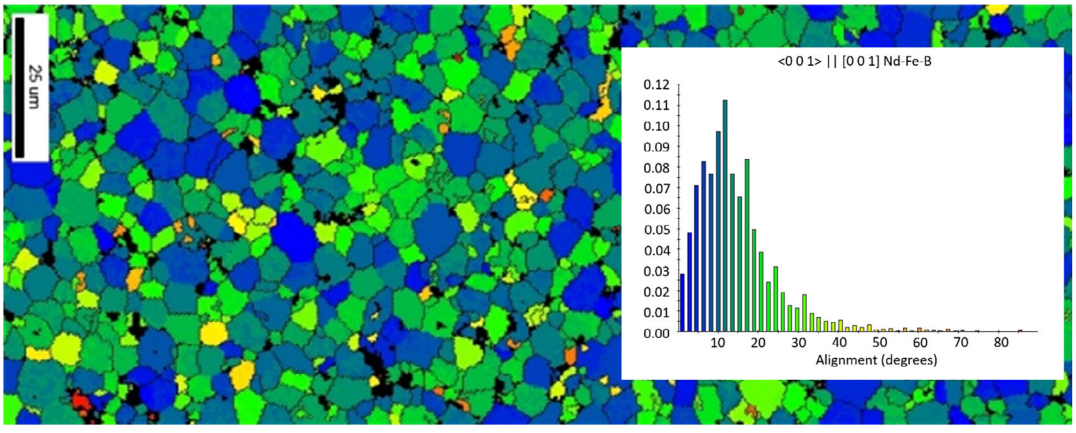

Figure 3. EBSD image of recycled Nd–Fe–B magnet. Inset shows the alignment distribution of the grains.

magnet heating during operation of the Halbach array at increased frequency can occur; thus, proper magnet design and adequate β are needed; otherwise, demagnetization effects can occur. Therefore, the materials with larger amounts of additives were selected to prevent demagnetization in the demonstrator magnet.

2.4. Suitability Analysis

The magnetic properties of the recycled materials shown in Table 1 are in the same range as commercially produced permanent magnets from new raw materials. The remanence of up to 1.4 T allows us to construct a Halbach system with a flux density above 1 T.

Rotatable Halbach cylinders can apply a large magnetic field to the magnets that make up the cylinders in the antiparallel state. This can lead to demagnetization of these magnets and to a loss of performance.

The high coercivity of at least 1.3 T ensures that this cannot happen with the recycled magnets used here. Therefore, the application of recycled magnets, with their lower environmental footprint, is technically feasible for magnetocaloric cooling applications.

2.5. The Economics of Recycling Nd–Fe–B Magnets

The magnets produced via the M2M recycling route have excellent properties that are equal to or surpass those of magnets produced from other recycling route,[21] or from new raw materials.[25–27]

The cost of producing the recycled permanent magnets used in this work has been evaluated via life cycle analysis, energy consumption evaluation, and a substantial literature review of available data. It has been shown that a 46% saving in energy consumption is achieved when following the M2M route, whereas more than 11 tons of CO_2 for every ton of magnet produced are sequestrated from the environment when comparing against the virgin magnet manufacturing route.[19] Energy consumption and environmental impact is directly correlated to operating costs; therefore, a reduction in energy consumption and carbon footprint increases profitability. If to this we add the environmental costs associated with RE mining and the negative externalities experienced by the communities exposed to the radioactive waste, it is obvious that the M2M recycling process is economically and environmentally desirable.[21]

A comprehensive LCA analysis comparing a real industrial scale M2M Nd–Fe–B magnet against a traditional first-use magnet shows that the former offers a substantially lower environmental and economic impact on all ten impact categories analyzed. Striking differences come from the analyzed impact on water acidification, global warming, and carcinogenic chemicals emissions, for which the impact of the M2M route versus the virgin route is 20% or more lower than the virgin route[32]

In addition, the M2M process is the only enabler of reverse logistic solutions that allows waste magnets to enter back into the supply chain. The supply of end-of-life magnets coming either from hard disk drive or hybrid electric vehicle/electric vehicle exceeds 1000 and 2000 t year^{-1}, respectively. Magnets from end-of-life application are fed back into the supply chain and are acquired at a discounted value compared with RE metal markets creating material cost efficiencies within the M2M production process, as well.

Recycling RE permanent magnets and their role in a circular economy will evolve with better collection programs and new harvesting technologies over time. This can shift the economics in favor of recycling magnet-containing products when compared with the traditional extraction of RE materials from the ground.

One other point that is worth considering is the impact of future legislation. It is very possible that we could see recycling being legally enforced, for example, with products for sale having to contain a minimum quantity of recycled components or materials, or in some cases products would have to be produced from materials sourced within a certain geographical region for strategic reasons. This could mean that the recycling of magnets will become economically even more attractive due to the introduction of national or international legislation.

3. Magnetocaloric Material La–Fe-Mn–Si

A good magnetocaloric material needs to exhibit a number of key properties.[33,34] First, the material needs to have a large adiabatic temperature and entropy change. In addition, the heat conductivity of the material needs to be as high as possible to efficiently remove the heat generated by the MCE. From the engineering point of view, magnetocaloric materials need to be mechanically and chemically stable and shapeable to form a variety of structures. From an economic perspective, the material needs to be cheap, it should have a low RE content, and it needs to be commercially available to be applied in cooling applications on a very large scale.[5–7,35]

In the following, these properties will be discussed when using La–Fe–Mn–Si spheres with seven different working temperatures, i.e., Curie temperatures, which were supplied by Vacuumschmelze GmbH, Germany. The material is charged with hydrogen and doped with manganese to give it superior magnetocaloric properties around room temperature.[36]

3.1. Structural Properties

To investigate the microstructure and phase distribution of the particles, SEM and energy-dispersive X-ray spectroscopy (EDS) analyses were performed on selected La–Fe–Mn–Si particles, ($T_t = 18.8\,^{\circ}C$). An overview of the size and shape of the particles is shown in **Figure 5**.

In general, well-synthesized La–Fe–Mn–Si samples are dense bulk alloys and consist mainly of the primary phase ($NaZn_{13}$-structure) and have a small amount of secondary or ternary phases.[36–38]

Figure 6 shows the sample's microstructure, based on a) BSE overview image as well as a magnified BSE image, along with b) EDS point analysis spots. The corresponding EDS results are shown in **Table 2**.

From the SEM images, the commercial La–Fe–Mn–Si particles are less homogeneous than the samples described in the literature. The surfaces and the cores of the particles exhibit a high porosity of approximately 20% (black contrast). According to the higher-magnification image in Figure 6b, the sample consists of three phases, with a large amount of secondary phase. At spot 1,

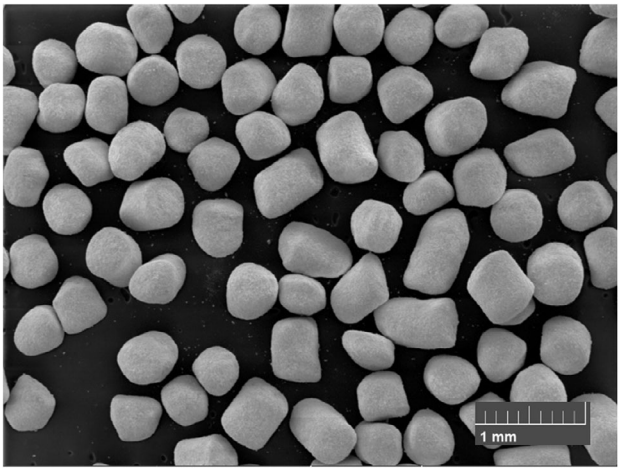

Figure 5. SEM image in SE mode of spherodized La–Fe–Mn–Si particles.

the primary La–Fe–Mn–Si, $NaZn_{13}$ phase was observed. In the case of the spherical particles, the secondary phase is not the $La_1Fe_1Si_1$ phase, as expected[37] but an Fe-rich phase (see Table 2, Spot 2). The problem of a large Fe content is that the material has a high residual magnetization above the transition temperature, which lowers the MCE as well as the efficiency for the refrigeration process.[37,39] In addition to that, the third phase (Spot 3) seems to be a La-oxide phase with some Fe content, which is not magnetic and reduces the magnetocaloric properties even more, due to the reduced magnetization.

Table 2. EDS analysis of LaFeSi.

Phase	Spot	La [at%]	Fe [at%]	Mn [at%]	Si [at%]	O [at%]
La_{13}(Fe, Mn, Si)	Spot 1	7.3	80.4	1.8	10.5	–
Fe-rich phase	Spot 2	0.4	91.9	2.6	2.6	–
La–Oxide phase	Spot 3	29.9	14.9	<0.1	2.5	48.4

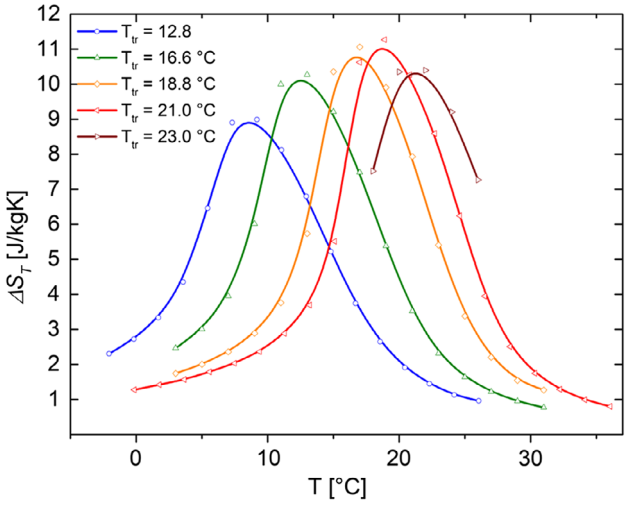

Figure 7. Magnetic entropy changes for five grades of hydrogenated La–Fe–Mn–Si.

3.2. Magnetocaloric Properties

To assess the magnetocaloric properties and correlate these with the microstructure, magnetization and adiabatic-temperature-change measurements were assessed for all five grades of particles. The isothermal entropy change was measured in a commercial PPMS system with an applied field of $\mu_0 H = 2\,\mathrm{T}$ in field steps of 0.2 T and is shown in **Figure 7**.

According to the obtained results, the maximum of the samples' magnetic entropy change ranges from 9 J kgK^{-1} (for $T_{tr} = 12.8\,^{\circ}\mathrm{C}$) and 11 J kgK^{-1} (for $T_{tr} = 21.0\,^{\circ}\mathrm{C}$), which is comparable to literature.[6,36,40]

The results for an applied field change of 1.0 and 1.9 T are shown in **Figure 8**. The samples consisted of compacted spheres bonded together with thermally conductive epoxy. The adiabatic temperature changes are almost similar for the different compositions. Nevertheless, the maxima are lower than 3 K and with this lower than for the best lab-produced La–Fe–Mn–Si samples from literature.[36,41–43]

In summary, the magnetocaloric properties of the commercially available samples are judged to be sufficient for use as heat exchangers in this study, and for understanding and improving the overall working principle of La–Fe–Mn–Si heat exchangers.

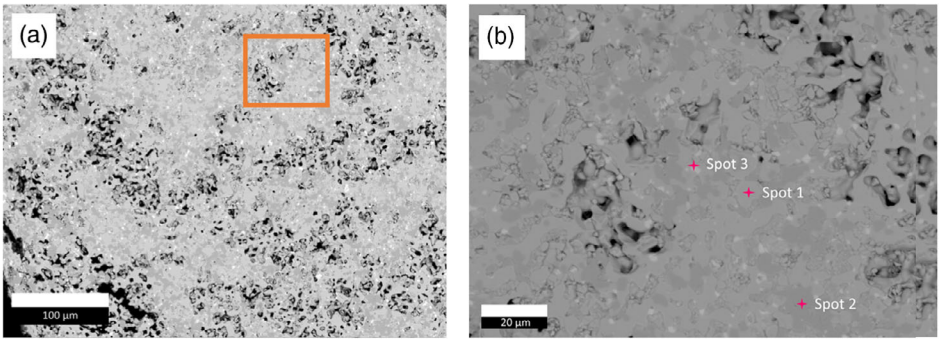

Figure 6. a) SEM BSE image of polished surface of spherodized La–Fe–Mn–Si particles in low and high resolution. b) EDS spots are marked, which are shown in Table 2.

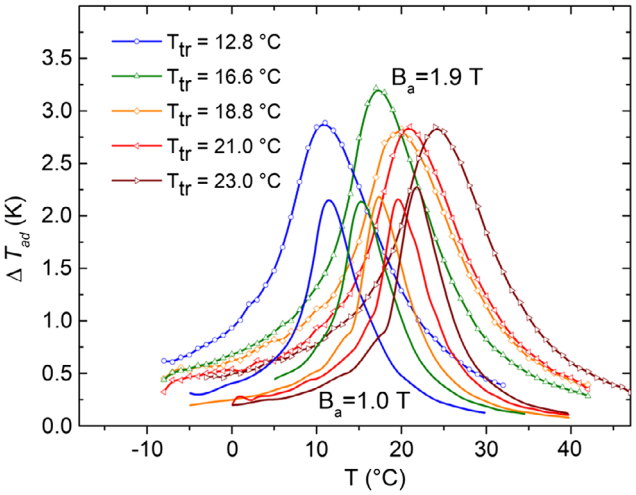

Figure 8. Adiabatic temperature change measurements for five La–Fe–Mn–Si samples in packed sphere shape, not corrected for demagnetization.

4. The Permanent Magnet Setup

4.1. Design Criteria of a Permanent Magnet Field Source

According to Kitanovski et al., four different magnet designs can be categorized:[7] a static or moving 2D magnet assembly, static and rotary 2D Halbach magnet assemblies, and 3D Halbach magnet assemblies.

We chose a rotary 2D Halbach design as it fits the prerequisites of having a large magnetic field in a large volume that is easily accessible to test different materials.

As mentioned previously, to reduce the ecological footprint of the MCE device, recycled Nd–Fe–B permanent magnets are used here to design an optimized Halbach setup.

4.2. Optimization Procedure for the Halbach Magnet

Bjørk et al.[44–46] proposed the parameter Λ_{cool} as a figure-of-merit for permanent magnet assemblies used in magnetic refrigeration and it is defined as

$$\Lambda_{cool} = \left(\left\langle B_{high}^{\frac{2}{3}} \right\rangle - \left\langle B_{low}^{\frac{2}{3}} \right\rangle \right) \frac{V_{MCM}}{V_{Mag}} P_{field} \tag{1}$$

B_{high} and B_{low} are the highest and lowest magnetic flux densities that the magnetocaloric material experiences during a cycle. V_{MCM} and V_{Mag} correspond to the volume of the magnetocaloric material and the permanent magnet material. P_{field} is the fraction of a cycle during which the magnetocaloric material experiences the high magnetic field. The brackets $\langle \dots \rangle$ indicate that the respective volume average needs to be considered.

The parameter Λ_{cool} is however less useful as an optimization goal function for nested Halbach cylinders which we chose in our setup, because it tends to be higher for very small magnets, which can be derived from the formula for the magnetic flux density in an infinitely long Halbach cylinder B_{inf}

$$B_{inf} = B_r \ln \frac{r_o}{r_i} \tag{2}$$

and the volume of the magnet and the magnetocaloric material, which is

$$V_{mag} = \pi \left(r_o^2 - r_i^2 \right) L \tag{3}$$

$$V_{MCM} = \pi r_i^2 L \tag{4}$$

Here B_r is the remanent flux density of the material used, r_o and r_i are the inner and outer radii of the cylinder and L is the length of the cylinder. In an ideal case, where the entire volume of the cylinder can be filled with the magnetocaloric material and B_{low} is 0, we obtain

$$\frac{\Lambda_{cool}}{P_{field}} = B_r^{\frac{2}{3}} \left(\ln \frac{r_o}{r_i} \right)^{\frac{2}{3}} \frac{r_i^2}{r_o^2 - r_i^2} \tag{5}$$

This term goes to infinity as r_o approaches r_i. Usual optimization routines use boundaries to avoid too extreme geometries, but the fact that $\frac{\Lambda_{cool}}{P_{field}}$ goes to infinity for thin Halbach cylinders means that an optimization routine always yields the smallest possible geometry within the given boundaries, which can be seen in ref. [47].

To avoid this problem, we used a generalized approach for a suitable figure-of-merit for the optimization of the geometry

$$D_{cool\$} \sim \frac{MCE}{Cost} \tag{6}$$

MCE is the total amount of MCE that is achievable in the design (for example, the total in entropy change in JK^{-1}). We assume that it is equal to the case in Equation (1).

Cost can be any generalized type of price that has to be paid to achieve the MCE. It can simply be the cost of the raw materials used for the device, or if the overall volume is considered to be a factor, this volume can also be associated with the price.

In this study, the cost is the volumetric price of the magnetic and magnetocaloric material multiplied by the volume of the material. Depending on the goal of the optimization, other cost functions could also be applied here, for example, the ecological footprint or the CO_2 equivalent to produce these materials. In addition, if a lightweight device is preferred, it is possible to add some terms that punish large, heavy devices.

For the optimization procedure, the machining costs are neglected because they do not depend greatly on the geometrical dimensions.

This general approach can still be applied in a more application-oriented device. There the cost has to include auxiliary components as well as the core magnet itself. However, it would make the whole optimization process less automatic, which is why we neglected it in this work.

In our case, we obtain

$$D_{cool\$} = \left(\left\langle B_{high}^{\frac{2}{3}} \right\rangle - \left\langle B_{low}^{\frac{2}{3}} \right\rangle \right) \frac{V_{MCM} P_{field}}{P_{Mag} \cdot V_{Mag} + P_{MCM} \cdot V_{MCM}} \tag{7}$$

with P_{Mag} and P_{MCM} as the volumetric price of the magnet and our magnetocaloric material.

Table 3. Comparison of different magnet systems from ref. [44].

Reference	Type	V_{mag} [cm^3]	V_{MCM} [cm^3]	B_{high} [T]	B_{low} [T]	P_{field}	D_{cool} [T^2/3/€) × 10^{-5}
This work	nested Halbach cylinder	520	63.6	1.15	0.02	0.5	7.7
Engelbrecht[48]	Halbach cylinder	500	70	1.03	0	0.5	8.1
Kim and Jeong[49]	Halbach cylinder	200	10	1.4	0	0.5	3.8
Lu[50]	Halbach cylinder	2940	140	1.4	0	0.5	3.6
Tura and Rowe[51]	nested Halbach cylinder	1030	50	1.4	0.1	0.5	3.1

The main advantages of this parameter in comparison to Λ_{cool} as an optimization goal is that it balances the gain of the magnet and the magnetocaloric material against their costs, and the only artificial optimization limit that needs to be set is the budget. For the calculation shown in **Table 3**, we estimated a material price of 100€/kg which is based on the price estimated by the material manufacturer when mass produced.

4.3. Optimization Procedure

The optimization parameters were the ratio of the inner and outer radii of the two cylinders and the ratio of the lengths of the cylinders to the outer radii. The inner radius of the inner cylinder was set to 30 mm, due to the machining constraints of our pumping system, and the upper bound was set to 90 mm, due to machining constraints of the magnet manufacturer. The inner radius of the outer cylinder was calculated on the basis of the gap between the cylinders that is necessary for the housing of the permanent-magnet material. Most other optimization routines set a goal for a desired magnetic field and calculate the best geometry for that field. We follow a different approach here: We set geometrical constraints given by our budget and calculate the best geometry and the best magnetic field change that is achievable with a given budget.

The magnetic field density for each cylinder was calculated in the center of the cylinder according to[12]

$$B = B_r\left(\ln\frac{r_o}{r_i} + \frac{L}{4}\left(\frac{1}{\sqrt{\frac{L^2}{4}+r_i^2}} - \frac{1}{\sqrt{\frac{L^2}{4}+r_o^2}}\right) - \ln\frac{\frac{L}{2}+\sqrt{\frac{L^2}{4}+r_o^2}}{\frac{L}{2}+\sqrt{\frac{L^2}{4}+r_i^2}}\right) \tag{8}$$

The value for $B_r = 1.3$T, a value achievable with the UMC's recycled Nd–Fe–B magnets.

The magnetic field of the cylinders was calculated for each set of parameters. It was assumed that the magnetocaloric material is as expensive as the permanent magnet, because the production route and equipment for production of La–Fe–Si and Nd–Fe–B are similar.

With this information $D_{cool\$}$ was evaluated. For a given budget, the optimal geometry was found, and the given parameter set stored.

The chosen geometry is summarized in **Table 4**.

The resulting magnet system and the optimization parameter is compared with other Halbach-based magnet systems from literature[42] in Table 4. The proposed setup is the best nested Halbach cylinder and only slightly worse than a similar single Halbach cylinder in terms of the chosen optimization parameter.

Table 4. Geometry of the magnets for the Halbach setup.

	Inner radius [mm]	Outer radius [mm]	Length [mm]
Inner Halbach magnet	15.0	24.2	90
Outer Halbach magnet	29.2	48.3	90

4.4. Assessment of Magnetic Performance

The resulting geometry was simulated with COMSOL Multiphysics to estimate the 3D field distribution. The UMC then produced the Halbach cylinders from recycled Nd–Fe–B material. The total mass of Nd–Fe–B was $m_{mag} = 3.9$ kg.

The magnetic flux density of the assembled cylinders was measured along the axis of the cylinder in the center for different alignments of the cylinders with a 3D Hall probe and compared with the simulation, as shown in **Figure 9**.

4.5. Setup of the Magnetic Cooling Unit

The magnetocaloric cooling demonstrator consists of a DC power supply for the driving electromotor. It is coupled by gears to a cylindrical pump and to the inner Halbach cylinder. This ensures

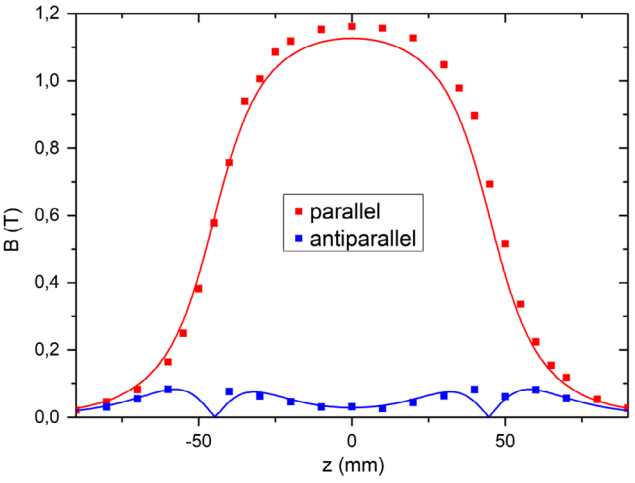

Figure 9. Magnetic field along z axis for parallel and antiparallel alignment of the cylinders. Dots are measured values; the lines are calculated with COMSOL.

Table 5. Key properties of the device.

Property	Value
Field change (max)	0.95 T (1.15 T)
Mass of magnet	3.9 kg
Active volume	63.6 cm^3
Usable volume	25 cm^3
Frequency	up to 5 Hz
Fluid	water
Temperature span	Up to 33 K
Maximum mass of Gd	120 g

the important synchronous operation of the fluid and the magnetic field without any electronic control and a net fluid flow of 0. The key properties of the device are summarized in **Table 5**.

The temperature is measured with thermocouples which are incorporated in the regenerator beds and connected to a data-acquisition computer. A summary of the key properties of the device are given in Table 4. A photograph can be seen in **Figure 10** and a schematic in **Figure 11**. A working scheme of the magnet and the piston at a frequency of 1 Hz is shown in **Figure 12**. The magnet and the piston are rotated by the same electromotor and are perfectly synchronized with a gear system connecting both. The phase shift φ between piston and magnet and the piston stroke are adjustable.

Preliminary experiments were performed to find the optimum phase shift and stroke and the results in the following section use always the best parameters.

5. Assessment of La–Fe–Mn–Si-Based Spherical Bed Heat Exchangers

To assess the performance of a magnetocaloric material in a cooling prototype, additional factors other than the adiabatic temperature change and the isothermal entropy change need to be considered. In a magnetic cooling machine, the material will operate under neither ideal adiabatic nor isothermal conditions. This contrasts with the measurements of the isothermal entropy change in Figure 7 and the adiabatic temperature change in Figure 8.

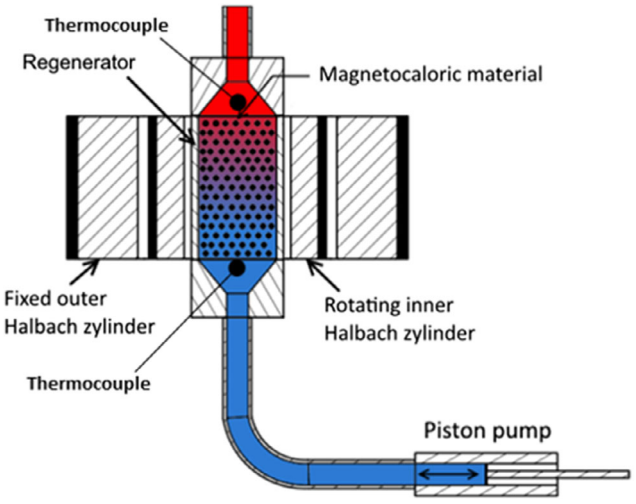

Figure 11. Schematic drawing of the magnetocaloric device.

The measurements in this section were performed with our magnetic cooling demonstrator. The different material samples were filled into a cylindrical compartment and temperature sensors were attached at both ends of the compartment. The compartments were put into the inner bore of the Halbach cylinders and attached to a piston pump which is shown in Figure 11.

5.1. Single-Stage Regenerator

First, a single-stage active magnetic regenerator ($T_{tr} = 23.0\,^{\circ}C$) was measured at different starting temperatures T_s. The magnetocaloric material's transition temperature is approximately room temperature, to avoid a large influence from the surrounding heat load.

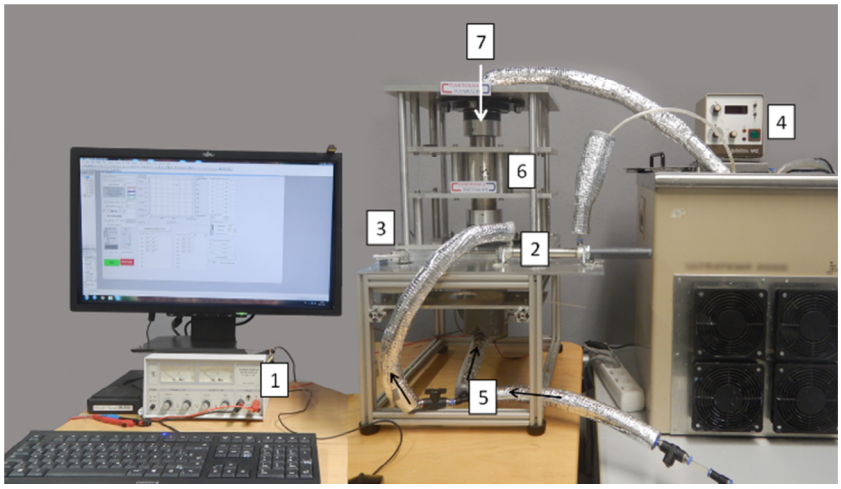

Figure 10. Magnetocaloric demonstrator with components: 1) Power supply for electro motor; 2) water pump; 3) setting for phase difference; 4) water reservoir with heating and cooling conditioner; 5) water hosepipes; 6) recycled Halbach-magnet; 7) regenerator insert.

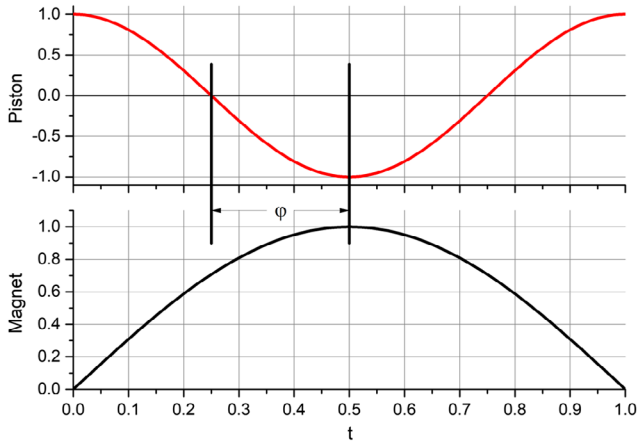

Figure 12. Working scheme of the demonstrator with the phase shift φ between the piston and the magnet.

The starting temperatures were varied from 17 to 27 °C, every 1 K step. The results are shown in **Figure 13** and are colored differently, according to the legend's description. Overall, the thermal span after 10 min is roughly the same for every measurement (TS ≈ 8 K). This confirms that only the surrounding temperature is important for the overall performance of the material and not the starting temperature.

5.2. Stacked Heat Exchanger

The thermal span of first-order transition materials such as La–Fe–Mn–Si is limited to the width of the transition temperature.[7,35] To overcome this problem, a reasonable alternative is to build graded heat exchangers, which consists of multiple parts constructed from materials with different transition temperatures.[52] A recent overview of studies on graded regenerators can be found in ref. [53].

To test the stackability, we constructed four different devices with 1, 2, 3, and 5 stages, consisting of La–Fe–Mn–Si materials with different T_{tr} values. The total volume of material used was kept the same as in the previous experiment.

The following active heat exchangers were prepared: 1) 1 Part: $T_{tr} = 18.8$ °C; 2) 2 Parts: $T_{tr} = 23.0/18.8$ °C; 3) 3 Parts: $T_{tr} = 23.0/18.8/16.6$ °C; 4) 5 Parts: $T_{tr} = 23.0/21.0/18.8/16.6/12.8$ °C.

The measurement results are shown in **Figure 14**. As a first step, from a single material to a double stack, the thermal span is increased by approximately 5 K. The heating curve is not improved, but the cooling curve is, as the added magnetocaloric material has a higher transition temperature with $T_{tr} = 23.0$ °C.

The idea of a graded magnetocaloric-material stack is that each compartment is working individually near its transition temperature, creating a thermal span. If multiple compartments are joined together, each one creates an increased temperature above and colder temperature below. If the transition temperature of the neighboring compartments is chosen correctly, they can function in the given regime and create a temperature difference on their own, which then again affects the other neighboring compartments, such as a cascade.

The triple stack is built by adding two magnetocaloric materials to the reference main compartment (18.8 °C). One with a higher (23.0 °C) and one with a lower (16.6 °C) transition temperature. Accordingly, the working temperature is extended, and the thermal span is increased from 8.1 K up to 19.5 K. As a result, the final temperatures of the hot and cold sides end up being higher and lower (see the green curve in Figure 14).

For the five-compartment stack, the addition of the 21.0 °C compartment has basically no influence, because the previous total temperature range is not extended to higher values. In contrast, the addition of one compartment with a lower transition temperature (12.8 °C) leads to an extension of the working range to lower temperatures, as well as to a lower final temperature (see the difference in the cooling of the green and blue curves in Figure 14).

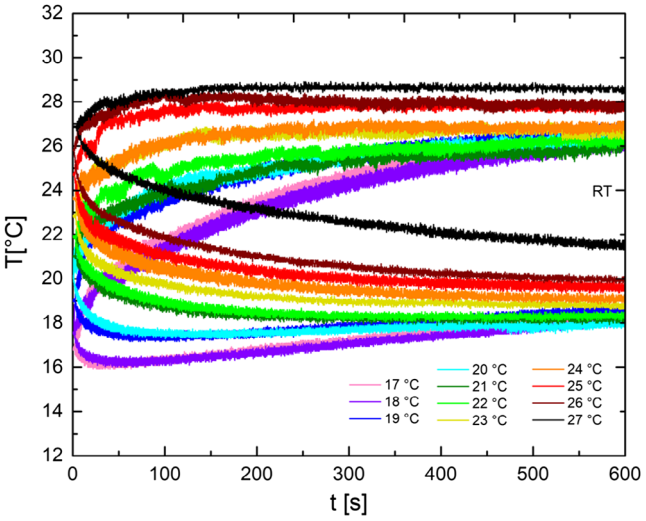

Figure 13. Comparison of the thermal span behavior of a single heat exchanger ($T_{tr} = 23$ °C), concerning different starting temperatures.

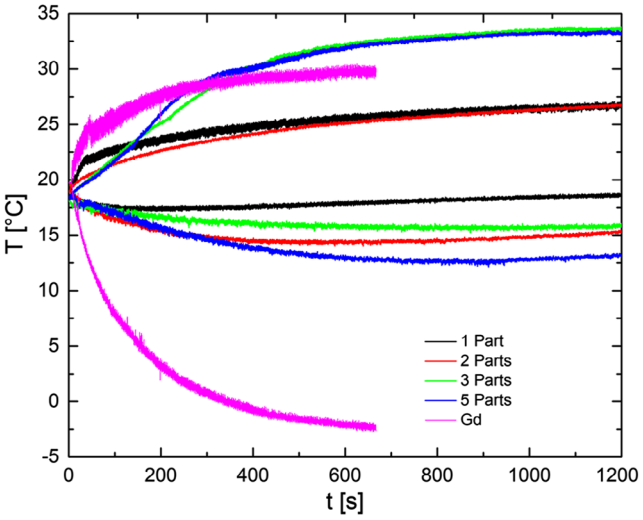

Figure 14. Comparison of the thermal span of different graded heat exchangers (1 Part, 2 Parts, 3 Parts, 5 Parts, and Gd).

Overall, the idea of building a graded La–Fe–Mn–Si heat exchanger, with certain steps in transition temperatures, is a very promising technique. With this, the working temperature range as well as the resulting thermal span can be increased significantly. For comparison, the results from a heat exchanger prepared from Gd with transition temperatures of 19 °C are also plotted in Figure 14. Here, a thermal span of 33 °C could be achieved. One can directly observe that for using first-order materials other than second-order materials such as Gd, one must prepare heat exchanger with more different stacks of materials with a different T_{tr}. This lies in the nature of the transition, as the first-order transition is usually much sharper than a second-order transition resulting in a narrower working range of the material.

In general, however, we could show that stacked La–Fe–Mn–Si heat exchangers present a reasonable and environmental-friendly alternative compared to Gd.

6. Characterization and Calculation Techniques

The SEM images and EDS analysis of the recycled magnets shown in Section 3 were made on a TESCAN Maija 3 SEM equipped with an EDAX Octane Plus EDS detector. The magnetic hysteresis loops at different temperatures were recorded using a METIS measurement system with a magnetic field change of 6.9 T. We used cylindrical samples and corrected the hysteresis loops for demagnetization. Prior to every measurement, the temperature was kept constant for 10 min to ensure a homogeneous temperature of the magnets.

The MCE material was characterized in a commercial Quantum Design PPMS system. The $M(T)$ curves were recorded with a sweep rate of 2 K min^{-1} at different fields. The isothermal entropy change ΔS_T was calculated from the $M(T)$ curves at different fields up to 2 T in field steps of 0.2 T.[54] The adiabatic temperature ΔT_{ad} change was recorded with a purpose-built device using a field change of 1.93 T.[55]

To optimize the geometry of a cylindrical Halbach array, as described in Section 5, the function fminsearch from scilab was used. It applies the Nelder–Mead algorithm[56] and is able to search for the unconstraint minimum of a given cost function. The 3D magnetic-field simulations were made using COMSOL multiphysics.

To assess the performance of the magnetocaloric materials under realistic conditions in Section 6, the spherical magnetocaloric material was packed into a closed tube made from polyoxymethylene with an inner diameter of 19 cm. The material was then retained in the tube by gluing small plastic sieves with a mesh diameter of 300 μm on the end of the tubes. Measurements were performed at a magnet-rotation speed of 1 Hz, with a total pumping volume for the water of 1.04 cm^3 in the device described in Section 4. The temperature at the bottom and the top of the active magnetocaloric heat exchanger was measured with T-type thermocouples glued onto the sieves.

7. Conclusions

We have successfully demonstrated the feasibility of building a "green" magnetic cooling device. We were able to show that conventional Nd–Fe–B magnets can be replaced by recycled magnets. The properties of the magnets prepared using the powder-metallurgy route are well suited in terms of their magnetic, thermal, and structural properties. In addition, we could show that La–Fe–Mn–Si is an effective replacement for gadolinium. By stacking La–Fe–Mn–Si materials with different T_{tr} temperature spans, a wide working temperature could be achieved. However, commercialization of these types of materials in a cooling device will require more time. The stacking of five materials was shown here, but to achieve a temperature span that is as high as for Gd, even more stacks are needed. Multiple issues relating to making good, long-term-stable magnetocaloric materials still need to be addressed, as the used La–Fe–Si was not able to reproduce the results several months after the experiments shown here. The use of recycled magnets makes clear sense in ecological terms, but the price of the magnets might still be too high for a mass-market product.[57] At the same time, it is clear that current prices of primary RE metals do not reflect real costs as social and ecological consequences of mining are not priced in. Here, legislation in China, but more importantly outside China (compare phase out of HFCs in EU) can change the economics quickly.

Acknowledgements

This work was supported by the European Research Council (ERC) under the European Union's Horizon 2020 research and innovation programme (grant no. 743116 project Cool Innov), the DFG (SPP 1599 Ferroic Cooling) and the Darmstadt Graduate School of Excellence Energy Science and Engineering (grant no. GSC 1070). Thanks go also to Gojmir Furlan at Urban Mining Company for building the magnetic assembly.

Conflict of Interest

The authors declare no conflict of interest.

Keywords

active magnetic regenerators, Halbach arrays, magnet recycling, magnetic cooling, magnetocaloric materials

Received: August 27, 2019
Revised: March 17, 2020
Published online: June 5, 2020

[1] M. Isaac, D. P. van Vuuren, *Energy Policy* **2009**, *37*, 507.
[2] S. Fähler, V. K. Pecharsky, *MRS Bull.* **2018**, *43*, 264.
[3] G. J. M. Velders, D. W. Fahey, J. S. Daniel, S. O. Andersen, M. McFarland, *Atmos. Environ.* **2015**, *123*, 200.
[4] C. B. Vining, *Nat. Mater.* **2009**, *8*, 83.
[5] O. Gutfleisch, M. A. Willard, E. Brück, C. H. Chen, S. G. Sankar, J. P. Liu, *Adv. Mater.* **2011**, *23*, 821.
[6] O. Gutfleisch, T. Gottschall, M. Fries, D. Benke, I. Radulov, K. P. Skokov, H. Wende, M. Gruner, M. Acet, P. Entel, M. Farle, *Philos. Trans. R. Soc. A* **2016**, *374*, 20150308.
[7] A. Kitanovski, J. Tušek, U. Tomc, U. Plaznik, M. Ozbolt, A. Poredoš, *Magnetocaloric Energy Conversion: From Theory to Applications*, Springer, Cham **2014**.
[8] S. Fähler, *Energy Technol.* **2018**, *6*, 1394.
[9] R. Gauß, G. Homm, O. Gutfleisch, *J. Ind. Ecol.* **2017**, *21*, 1291.

[10] J. Lyubina, O. Gutfleisch, M. D. Kuz'min, M. Richter, *J. Magn. Magn. Mater.* **2008**, *320*, 2252.
[11] F. Scheibel, T. Gottschall, A. Taubel, M. Fries, K. P. Skokov, A. Terwey, W. Keune, K. Ollefs, H. Wende, M. Farle, M. Acet, O. Gutfleisch, M. E. Gruner, *Energy Technol.* **2018**, *6*, 1397.
[12] H. Zijlstra, J. Philips, *Research* **1985**, *40*, 259.
[13] Y. Yang, A. Walton, R. Sheridan, K. Güth, R. Gauß, O. Gutfleisch, M. Buchert, B.-M. Steenari, T. Van Gerven, P. T. Jones, K. Binnemans, *J. Sustainable Metall.* **2017**, *3*, 122.
[14] B. Monfared, R. Furberg, B. Palm, *Int. J. Refrig.* **2014**, *42*, 69.
[15] R. Luglietti, P. Rosa, A. Pastore, S. Terzi, M. Taisch, *Proc. Manuf.* **2017**, *8*, 231.
[16] Roskill Information Services **2018**, https://roskill.com/market-report/rare-earths/ (accessed: February 2017).
[17] D. Benke, J. Wortmann, M. Pabst, T. Gottschall, I. Radulov, K. Skokov, O. Gutfleisch, D. Prosperi, A. Bevan, S. Dove, *MagnNews*, **2017**, pp. 24.
[18] M. D. Kuz'min, K. P. Skokov, D. Y. Karpenkov, J. D. Moore, M. Richter, O. Gutfleisch, *Appl. Phys. Lett.* **2011**, *99*, 012501.
[19] Mitsubishi Quietly Cleans Up Its Former Refinery, https://www.nytimes.com/2011/03/09/business/energy-environment/09rareside.html (accessed: February 2017).
[20] M. Zakotnik, C. O. Tudor, L. T. Peiró, P. Afiuny, R. Skomski, G. P. Hatch, *Environ. Technol. Innov.* **2016**, *5*, 117.
[21] M. Zakotnik, C. O. Tudor, *Waste Manage.* **2015**, *44*, 48.
[22] R. Gauß, O. Gutfleisch, in *Rohstoffwirtschaft und gesellschaftliche Entwicklung: Die nächsten 50 Jahre* (Eds.: P. Kausch, J. Matschullat, M. Bertau, H. Mischo), Springer, Berlin, Heidelberg, **2016**, p. 99.
[23] K. P. Skokov, O. Gutfleisch, *Scr. Mater.* **2018**, *154*, 289.
[24] K. Binnemans, P. T. Jones, K. Van Acker, B. Blanpain, B. Mishra, D. Apelian, *JOM* **2013**, *65*, 846.
[25] H. Sepehri-Amin, T. Ohkubo, M. Zakotnik, D. Prosperi, P. Afiuny, C. O. Tudor, K. Hono, *J. Alloys Compd.* **2017**, *694*, 175.
[26] S. Shen, M. Tsoi, D. Prosperi, C. O. Tudor, S. K. Dove, A. I. Bevan, G. Furlan, M. Zakotnik, *J. Magn. Magn. Mater.* **2017**, *442*, 158.
[27] D. Prosperi, A. I. Bevan, G. Ugalde, C. O. Tudor, G. Furlan, S. Dove, P. Lucia, M. Zakotnik, *J. Magn. Magn. Mater.* **2018**, *460*, 448.
[28] A. Lixandru, P. Venkatesan, C. Jönsson, I. Poenaru, B. Hall, Y. Yang, A. Walton, K. Güth, R. Gauß, O. Gutfleisch, *Waste Manage.* **2017**, *68*, 482.
[29] A. W. Ivor Rex Harris, *Allan Walton, John Speight*, Oxford University Press, Oxford **2010**.
[30] K. Loewe, D. Benke, C. Kübel, T. Lienig, K. P. Skokov, O. Gutfleisch, *Acta Mater.* **2017**, *124*, 421.
[31] *Magnetic properties of magnetically hard materials at elevated temperatures - methods of measurement*, IEC, **1999**.
[32] H. Y. Jin, P. Afiuny, S. Dove, G. Furlan, M. Zakotnik, Y. Yih, J. W. Sutherland, *Environ. Sci. Technol.* **2018**, *52*, 3796.
[33] J. Lyubina, R. Schäfer, N. Martin, L. Schultz, O. Gutfleisch, *Adv. Mater.* **2010**, *22*, 3735.
[34] T. Gottschall, K. P. Skokov, M. Fries, A. Taubel, I. Radulov, F. Scheibel, D. Benke, S. Riegg, O. Gutfleisch, *Adv. Energy Mater.* **2019**, *9*, 1901322.
[35] A. Kitanovski, U. Plaznik, U. Tomc, A. Poredoš, *Int. J. Refrig.* **2015**, *57*, 288.
[36] M. Krautz, K. Skokov, T. Gottschall, C. S. Teixeira, A. Waske, J. Liu, L. Schultz, O. Gutfleisch, *J. Alloys Compd.* **2014**, *598*, 27.
[37] J. Liu, M. Krautz, K. Skokov, T. G. Woodcock, O. Gutfleisch, *Acta Mater.* **2011**, *59*, 3602.
[38] O. Gutfleisch, A. Yan, K. H. Müller, *J. Appl. Phys.* **2005**, *97*, 036102.
[39] J. Liu, J. D. Moore, K. P. Skokov, M. Krautz, K. Löwe, A. Barcza, M. Katter, O. Gutfleisch, *Scr. Mater.* **2012**, *67*, 584.
[40] V. Franco, J. S. Blázquez, J. J. Ipus, J. Y. Law, L. M. Moreno-Ramírez, A. Conde, *Prog. Mater Sci.* **2018**, *93*, 112.
[41] I. A. Radulov, D. Y. Karpenkov, K. P. Skokov, A. Y. Karpenkov, T. Braun, V. Brabänder, T. Gottschall, M. Pabst, B. Stoll, O. Gutfleisch, *Acta Mater.* **2017**, *127*, 389.
[42] I. A. Radulov, D. Y. Karpenkov, M. Specht, T. Braun, A. Y. Karpenkov, K. P. Skokov, O. Gutfleisch, *IEEE Trans. Magn.* **2017**, *53*, 1.
[43] K. P. Skokov, D. Y. Karpenkov, M. D. Kuzmin, I. A. Radulov, T. Gottschall, B. Kaeswurm, M. Fries, O. Gutfleisch, *J. Appl. Phys.* **2014**, *115*, 17A941.
[44] R. Bjørk, C. R. H. Bahl, A. Smith, N. Pryds, *Int. J. Refrig.* **2010**, *33*, 437.
[45] R. Bjørk, C. R. H. Bahl, A. Smith, N. Pryds, *J. Appl. Phys.* **2008**, *104*, 013910.
[46] R. Bjørk, A. Smith, C. R. H. Bahl, N. Pryds, *Int. J. Refrig.* **2011**, *34*, 1805.
[47] P. V. Trevizoli, J. A. Lozano, G. F. Peixer, J. R. Barbosa Jr, *J. Magn. Magn. Mater.* **2015**, *395*, 109.
[48] K. Engelbrecht, J. B. Jensen, C. R. Haffenden Bahl, *Strojniski Vestnik/J. Mech. Eng.* **2012**, *58*, 3.
[49] Y. Kim, S. Jeong, in *AIP Conf. Proc.* (Ed: J. G. Weisend), Vol. *1218*, American Institute of Physics, College Park, **2010**, pp. 87–94.
[50] D. Lu, X. Xu, H. Wu, X. Jin, in *Proc. of the 1st Int. Conf. on Magnetic Refrigeration at Room Temperature*, Montreux, Switzerland, **2005**, pp. 1–6.
[51] A. Tura, A. Rowe, in *Proc. of the 2nd Int. Conf. of Magnetic Refrigeration at Room Temperature*, Portoroz, Slovenia, **2007**, pp. 363–370.
[52] J. A. Barclay, W. A. Steyert, Google Patents **1982**.
[53] A. Kitanovski, *Adv. Energy Mater.* **2020**, *10*, 1903741.
[54] L. Caron, Z. Q. Ou, T. T. Nguyen, D. T. Cam Thanh, O. Tegus, E. Brück, *J. Magn. Magn. Mater.* **2009**, *321*, 3559.
[55] H. Jian, K. P. Skokov, M. D. Kuzmin, I. Radulov, O. Gutfleisch, *IEEE Trans. Magn.* **2014**, *50*, 1.
[56] J. A. Nelder, R. Mead, *Computer J.* **1965**, *7*, 308.
[57] O. Diehl, M. Schönfeldt, E. Brouwer, A. Dirks, K. Rachut, J. Gassmann, K. Güth, A. Buckow, R. Gauß, R. Stauber, O. Gutfleisch, *J. Sustainable Metal.* **2018**, *4*, 163.